Earthq Sci (2015) 28(1):49–57
DOI 10.1007/s11589-015-0109-0

RESEARCH PAPER

Characteristics of subsurface density variations before the 4.20 Lushan M_S7.0 earthquake in the Longmenshan area: inversion results

Songbai Xuan · Chongyang Shen · Hui Li · Hongtao Hao

Received: 24 November 2014 / Accepted: 12 January 2015 / Published online: 7 February 2015

Abstract The 4.20 Lushan M_S7.0 earthquake occurred on the southwest segment of the Longmenshan fault on 20 April 2013. Some meaningful information on the preparation and occurrence of this earthquake was found based on the dynamic variation of gravity (DVG). To examine the great progress of the Lushan earthquake, we obtained the density variation (DENV) derived from the DVG using the compact gravity inversion method in this article. The inversion results reveal three main findings: (1) the DENV in the crust in the Jinshajiang fault area changed from positive in 2010–2011 to negative in 2011–2012. (2) The DENV in the Xianshuihe fault area decreased continuously from 2010 to 2012. (3) The DENV of the uppermost mantle of South China decreased in 2010–2011 and increased in 2011–2012. We propose that the flow/expansion of the middle-lower crust beneath the Bayan Har block and Moho subsidence on the southwest margin of the Chuan-Dian block may have been the major causes of the Lushan earthquake.

Keywords Density variations · Gravity inversion · Deep progress · Lushan earthquake

S. Xuan
School of Geodesy and Geomatics, Wuhan University, Wuhan 430079, China
e-mail: song_bai_whu@163.com

S. Xuan · C. Shen · H. Li (✉) · H. Hao
Institute of Seismology, China Earthquake Administration, Wuhan 430071, China
e-mail: lihuieq@163.com

C. Shen
e-mail: scy907@163.com

H. Hao
e-mail: ldzlz@126.com

1 Introduction

On 20 April 2013, the Lushan M_S7.0 earthquake occurred in Lushan, Sichuan, China. It was a destructive earthquake striking on the Longmenshan fault almost 5 years after the 2008 Wenchuan earthquake. Unlike the Wenchuan earthquake, previous studies have suggested that the obvious surface rupture has not been found by geological investigation in the earthquake region (Xu et al. 2013; Lei et al. 2014). Displacement has not been observed around the central earthquake region, but has been found in the regions about 20 km NE and SW from the epicenter (Zhao et al. 2013). The mechanism leading to the occurrence of the Lushan earthquake remains hotly debated. Several studies have proposed that the Wenchuan earthquake hastened the occurrence of the Lushan earthquake (e.g., Xu et al. 2013; Shan et al. 2013). However, the Lushan earthquake is not believed to be the aftershock of Wenchuan earthquake (e.g., Zhan et al. 2013). Others suggests that it is the outcome of crustal shortening caused by collision and extrusion between the Bayan Har block and South China block (e.g., He et al. 2014), or the reactivation of the basement faults (Lu et al. 2014).

For investigating the subsurface progress, dynamic gravity variation (DVG) has been widely used to explain the preparation and occurrence of earthquakes, such as the Tangshan (Chen et al. 1979; Li and Fu 1983), Haicheng (Chen et al. 1979) and Wenchuan earthquakes (Shen et al. 2009; Zhu et al. 2010). Zhu et al. (2013) suggested that significant DVG anomalies appeared in the 2–3 years before the earthquake. Further, the DVG images obtained from gravimetry in 2010–2012 revealed some useful information underground (Zhu et al. 2013; Hao et al. 2015).

In this study, we obtained the density variations (DENVs) of the crust and uppermost mantle derived from

the DVG (2010–2011 and 2011–2012) in the eastern Tibetan Plateau using compact gravity inversion. Based on the inversion results, we analyzed the characteristics of the subsurface movements before the Lushan earthquake and the possible factors contributing to the Lushan earthquake.

2 Tectonic setting in brief

As the transition zone between the Bayan Har block of the Tibetan plateau and Sichuan basin of the Yangtze block, the NNE-SSW trending Longmenshan fault zone is composed of the Maoxian-Wenchuan thrust fault, Yingxiu-Beichuan thrust fault and Anxian-Guanxian thrust fault from northwest to southeast (Fig. 1). It is a NW to SE thrusting and dextral strike-slip fault zone. The crust thickness of the Bayan Har block on the northwest of the Longmenshan fault is about 57–64 km, and the thickness of the Sichuan basin on the southeast of the Longmenshan fault is about 40–45 km (Wang et al. 2010; Zhang et al. 2011). Eastward extrusion and enlargement of the Tibetan Plateau generated by the Indian-Asian plates collision make the Longmenshan uplift (Clark and Royden 2000; Shoenbohm et al. 2006).

In Longmenshan and its surrounding regions, crustal shortening (Molnar and Tapponnier 1975; Houseman and England 1993; Royden et al. 2008; Chatterjee et al. 2013), lateral extrusion along major strike-slip faults (Tapponnier et al. 1982, 2001) and ductile lower crustal flow (Clark and Royden 2000; Shoenbohm et al. 2006; Bai et al. 2010) are widely recognized. Resulting from eastward and southeastward movement and extrusion of the Bayan Har block, large areas of low-density, low-velocity and high-conductive anomalies were observed in the middle-lower crust in the eastern Tibetan Plateau (Wang 2003; Wang et al. 2007; Zhang et al. 2009, 2011; Bai et al. 2010; Jiang et al. 2012). On the margin of the Bayan Har block, crustal movements are very active. In this century, four major earthquakes with devastating effects, including the 2013 M_S7.0 Lushan earthquake in China, all struck on the margin of the Bayan Har block (Chen et al. 2011; Zhang and Engdahl 2013; He et al. 2014).

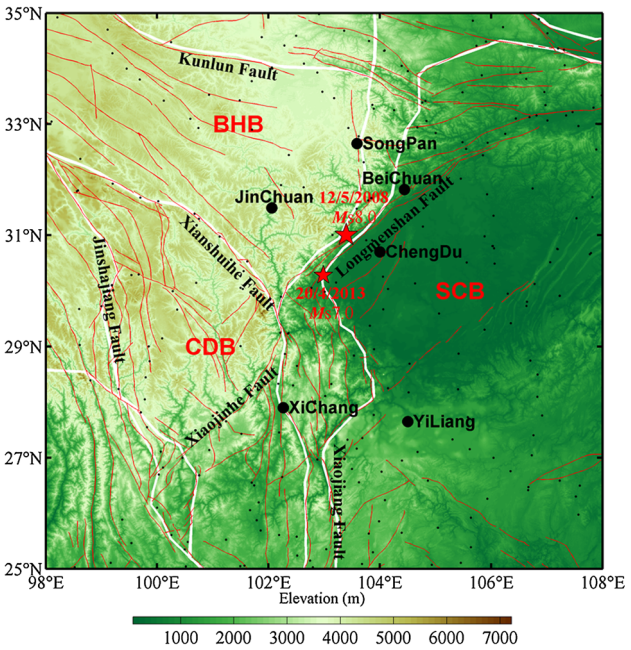

Fig. 1 Topography and tectonic setting around the Longmenshan area. The *black points* indicate the gravimetry locations. The *thin red lines* are faults. The *thick white lines* are the boundaries of the secondary blocks. The two *red stars* are the Wenchuan earthquake and Lushan earthquake. SCB, Sichuan Basin, CDB, Sichuan-Yunnan block, BHB, Bayan Har block

3 Data and method

3.1 DVG data

According to Hao et al. (2015), the DVG data used here are calculated by subtracting between the adjustment results at each point (Fig. 1) of the previous and later year from 2010 to 2012. DVG images ranging between −200 μGal (1 μGal = 10^{-8} m/s^2) and 200 μGal are shown in Fig. 2.

Figure 2a is the DVG image from 2010 to 2011. It illustrates the characteristics of the DVG 2 years before the Lushan earthquake on 20 April 2013. The most prominent feature in this map is that a NW-SE trending gradient belt is obvious in the middle of the northern area of the Chuan-Dian block (CDB). The negative DVG area is located to the northeast of the belt (<−100 μGal), and the positive DVG is located to the southwest of the belt (∼150 μGal). Moreover, the negative and low-amplitude positive DVG are almost separated by the LMSf between the Bayan Har block and Sichuan basin. The low-amplitude positive DVG (∼50 μGal) in the Sichuan basin is similar to the DVG before the 2008 Wenchuan earthquake (Shen et al. 2009; Zhu et al. 2010).

The DVG image from the year 2011 to 2012, 1 year before the Lushan earthquake, 2013, is shown in Fig. 2. The negative DVG played an important role in the study area, especially on both sides of the JSJf area (∼−200 μGal). In the region perpendicular to the Longmenshan fault across the epicenter of the Lushan earthquake, the DVG decreased (negative). As shown in Fig. 2a, the DVG in much of South China, including the Sichuan basin, was nearly invariable.

3.2 Method

In order to obtain crustal density variations, we use the method of compact gravity inversion proposed by Last and

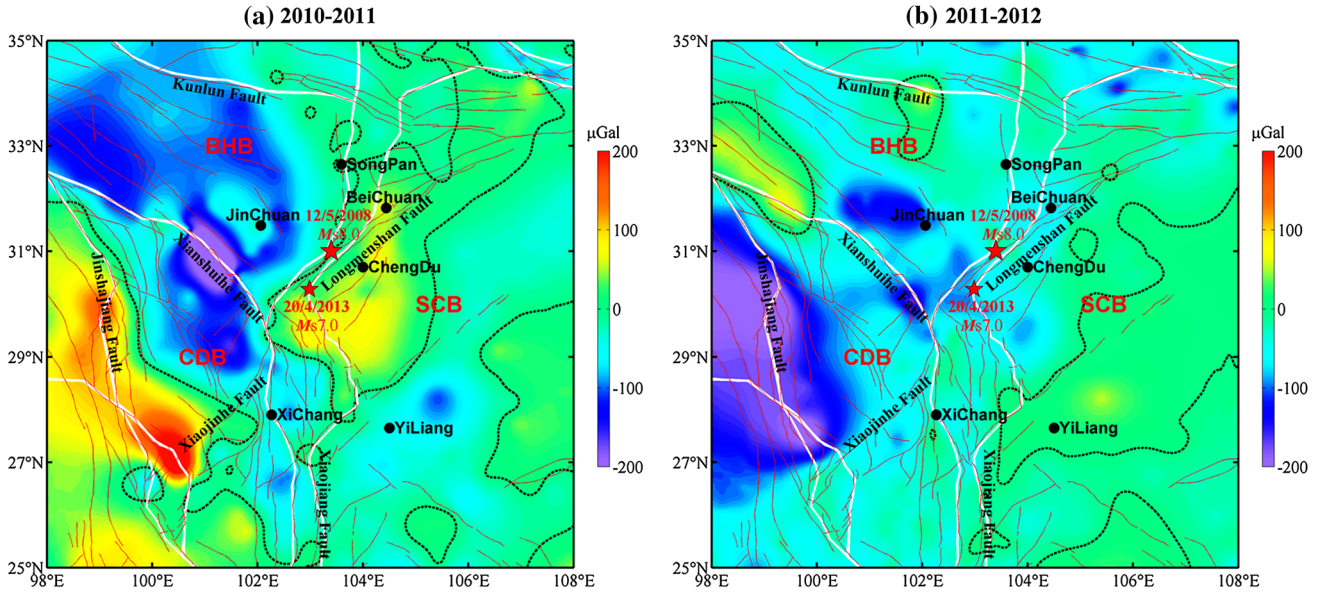

Fig. 2 The DVG of **a** 2010–2011 and **b** 2011–2012 (Hao et al. 2015). Note that the *dotted black lines* are 0 μGal contours

Kubik (1983) and developed by Barbosa and Silva (1994). This method is useful for detecting migrant abnormal bodies probably related to the earthquake.

In the model applied here, the subsurface domain is divided into numerous rectangular prisms. Then, with the distribution of density variations $\boldsymbol{V}$ in this model, the variations of gravity $\boldsymbol{G}$ using the matrix are given by

$$\boldsymbol{G} = \boldsymbol{A}\boldsymbol{V} + \boldsymbol{E}, \tag{1}$$

where $\boldsymbol{A}$ is the influence of all prisms on $\boldsymbol{G}$ with unit density variations; $\boldsymbol{E}$ is the noise matrix associated with the observation data. Finding V can be undertaken to minimize the function of the density variations and errors. It can be stated as function (2).

$$\sum_{j=1}^{M} w_{vj} v_j^2 + \sum_{i=1}^{N} w_{ei} e_i^2 \rightarrow \min, \tag{2}$$

subject to Eq. (1). Here, M is the number of prisms, N is the number of observation stations, $w_{vj} = f(v_j)/v_j^2$ is a density weighting function, and $w_{ei} = f(e_i)/e_i^2$ is a noise weighting function.

Solving $\boldsymbol{V}$ with the compact condition is a weighted least-squares problem, whose solution is

$$\boldsymbol{V} = \boldsymbol{W}_v^{-1}\boldsymbol{A}^T(\boldsymbol{A}\boldsymbol{W}_v^{-1}\boldsymbol{A}^T + \boldsymbol{W}_e^{-1})^{-1}\boldsymbol{G}, \tag{3}$$

where the weights $\boldsymbol{W}_v$ and $\boldsymbol{W}_e$ are the diagonal matrix composed of w_{vj} and w_{ei} respectively.

The inversion should be solved iteratively. We can define $\boldsymbol{W}_v$ and $\boldsymbol{W}_e$ at each step to implement the iteration. At the kth step, the weights $\boldsymbol{W}_v$ and $\boldsymbol{W}_e$ are defined by the outcome of the previous iteration

$$[\boldsymbol{W}_v^{(k-1)}]_{jj}^{-1} = [v_j^{(k-1)}]^2 + \varepsilon$$

and

$$[\boldsymbol{W}_e^{(k-1)}]_{ii}^{-1} = \sigma_0 \boldsymbol{D}_{ii}^{(k-1)} \boldsymbol{C}_0^{(k-1)} \{[e_{ii}^{(k-1)}]^2 + \eta\},$$

where ε and η should be chosen to be as small as possible; $\boldsymbol{D} = \boldsymbol{A}\boldsymbol{W}_v^{-1}\boldsymbol{A}^T$, σ_0 is the a priori signal-to-noise ratio.

More procedural details can be found in Last and Kubik (1983), and the constraints on the density variations can be found in Barbosa and Silva (1994).

4 Results

Redistribution of subsurface matter (namely density variations here), water storage variation and surface vertical deformation for local areas are the major factors in gravity change (Battaglia et al. 2003). The maximum rate of vertical deformation based on Hao et al. (2014) is 5.8 ± 1.0 mm/a, inferred from the leveling data, and the gravity effect of the vertical deformation is estimated to be about 1.78 μGal/a. Zhu et al. (2010) indicated that the hydrologic effects on the DVG in the study region, calculated from the GLDAS model, are in the range of 15–20 μGal. The sum of the effects caused by vertical deformation and hydrology was less than 25 μGal in the 2010–2012 period. For the DVG magnitude, we can consider that most DVG effects in this study are caused by redistribution of the subsurface matter.

The gravity data we used were in the area of 97°–112°E and 21°–42°N; therefore, for the study area of 98°–108°E

and 25°–35°N, we did not consider the boundary effects. The subsurface domain (the horizontal domain is 97°–112°E and 21°–42°N; the depth domain is 0–80 km) was divided into 10,664 prisms with a size of 50 km × 50 km × 10 km. The data for computations were obtained by subtracting the regional variations of gravity obtained by upward continuation at 160 km (Jacobsen 1987) from the data in Fig. 2. According to the experiments of Last and Kubik (1983), fewer than ten iterations were sufficient to achieve convergence, so ten was used for the maximum number of iterations. Based on the approximate formula $\Delta g = 2\pi G\Delta\rho h$, the range of the DENV is from −0.47 to 0.47 kg/m^3 for the DVG range in the study area; we used ±0.4 kg/m^3 for constraints of density variations. When the standard deviation (STDEV) was ≤5 μGal or after ten iterations, the iteration was stopped. At each step, the approximations of the first order DWT at each layer were used to smooth the density variations. The STDEVs of the two inversion results were 5.9 μGal and 4.6 μGal, respectively. Layered DENV images (six of eight) from 2010–2011 and 2011–2012 are shown in Figs. 3 and 4, respectively.

4.1 The DENV in 2010–2011

Near the surface, as shown in Fig. 3a (the 0–10-km layer, called the upper crust as well), the abnormal body with a positive DENV (∼0.1 kg/m^3) in the western part of the study area between 27°N and 31°N was almost consistent with the trend of JSJf. This suggests the upper crust moved to this area, which is consistent with the explanations of surface deformation derived from the GPS (Zhang et al. 2004; Gan et al. 2007; Wang et al. 2008).

The DENV for the middle crust layer (10–20 km) is shown in Fig. 3b. The negative DENV (<−0.1 kg/m^3) in the V-shaded area formed by the LMSf and XSHf indicated that the expansive matter of the Byan Har block was in a state of expansion. From the amplitude of the positive DENV (∼0.1 kg/m^3) in the southwest of the XSHf and in the Sichuan basin, extruded by the Bayan Har block, the southwestward was much more significant. In Fig. 3a, the positive DENV near JSJf reflects not only the effect of deformation, but also the effect of thrusting of the Bayan Har block.

At the depth of 20–50 km (Fig. 3c–e), the DENV of the major geological units in the middle-lower crust (Fig. 3e is the uppermost mantle for the Sichuan basin) obviously presented different characteristics. The negative DENV with a magnitude less than −0.1 kg/m^3 crossed over XSHf to the Chuan-Dian block but not LMSf, and the maximum appeared in the 40–50-km layer (Fig. 3e). The DENV (>0.1 kg/m^3) was positive near the JSJf area, and the maximum was in the 30–40-km layer (Fig. 3d). The positive DENV (∼0.1 kg/m^3) in the Sichuan basin should be caused by top-down extrusion of the Bayan Har block from NW to SE. An obvious negative DENV (<−0.1 kg/m^3) in the eastern area of the Xiaojiang fault (Fig. 3e) might be caused by the heat matter input (Bai et al. 2010).

The less obvious DENV (∼−0.05–0.05 kg/m^3) in the 50–60-km layer (Fig. 3f) indicated the tectonic impact on the uppermost mantle was small in 2010–2011.

4.2 The DENV in 2011–2012

The DENV on both sides in the 0–10-km layer (Fig. 4a) was negative. Its amplitude was comparable to the positive DENV shown in Fig. 3a.

In the middle-lower crust (Fig. 4b, 10–20 km layer), the negative DENV (<−0.1 kg/m^3) covered the northern Chuan-Dian block. As shown in Fig. 4c–e, the negative DENV (<−0.1 g/m^3) crossed over the southwest segment of the LMSf southwest of the epicenter of the 2008 Wenchuan earthquake and continuously decreased on both sides of the XSHf and the V-shaded area (Fig. 3c–e). The DENV was nearly invariable in other regions of the Bayan Har block. This phenomenon suggests that the expansion of the middle-lower crust beneath the Bayan Har block continued. Around the epicenter of the Lushan earthquake was the new area within the larger negative DENV (≤100 g/m^3) at a depth of 20–50 km (Fig. 4c–e). This may be the sign of the occurrence of the Lushan earthquake.

The NE-SW trending positive DENV (40–50-km layer, Fig. 4e) in the uppermost mantle had been separated to the eastward and southward part, respectively (50–60-km layer, Fig. 4f), beneath South China.

In summary, the most obvious DENV appeared in the area northwest of the line of Longmenshan-Xiaojinhe and along the Xianshuihe fault in the middle-lower crust from 2010 to 2012.

5 Discussion and conclusions

Here we explain the dynamic characteristics of the subsurface mass before the Lushan earthquake. Although our inversion results are an interpretation model, it is not the true density change in the subsurface. Many parameters and influences on the DVG have not yet been considered. This model has implications for understanding this progress.

Because of the resistive Sichuan basin, the directions of eastward movement (Zhang et al. 2004; Gan et al. 2007; Wang et al. 2008) and matter flow (Clark and Royden 2000; Clark et al. 2005; Shoenbohm et al. 2006; Klemperer 2006; Bai et al. 2010) of the Bayan Har block have been changed to north, south and southwest, including upward and downward expansion under the Longmenshan region (Fig. 5). For inhomogeneous distribution of the interior

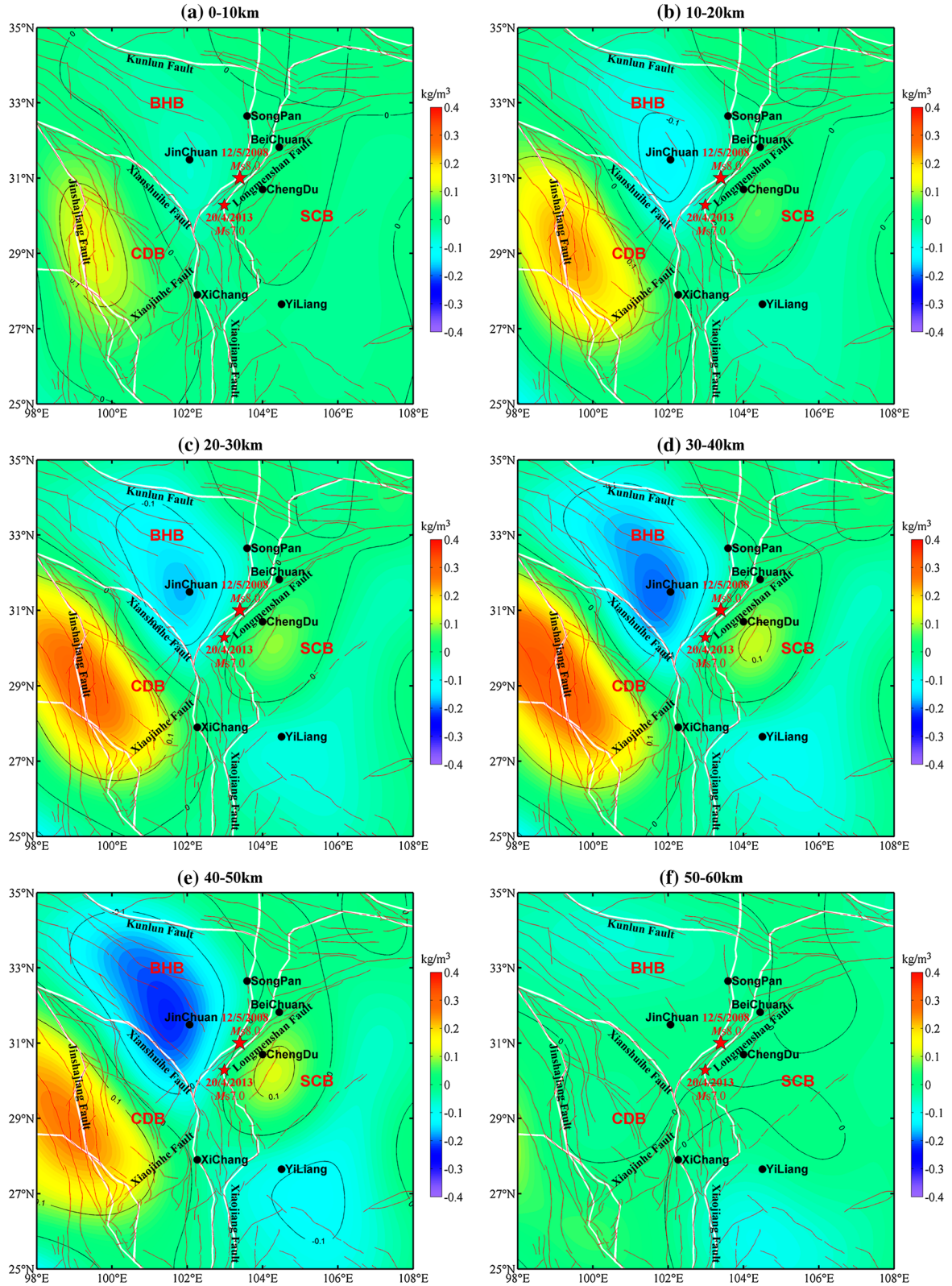

Fig. 3 DENV in 2010–2011 derived from Fig. 2a

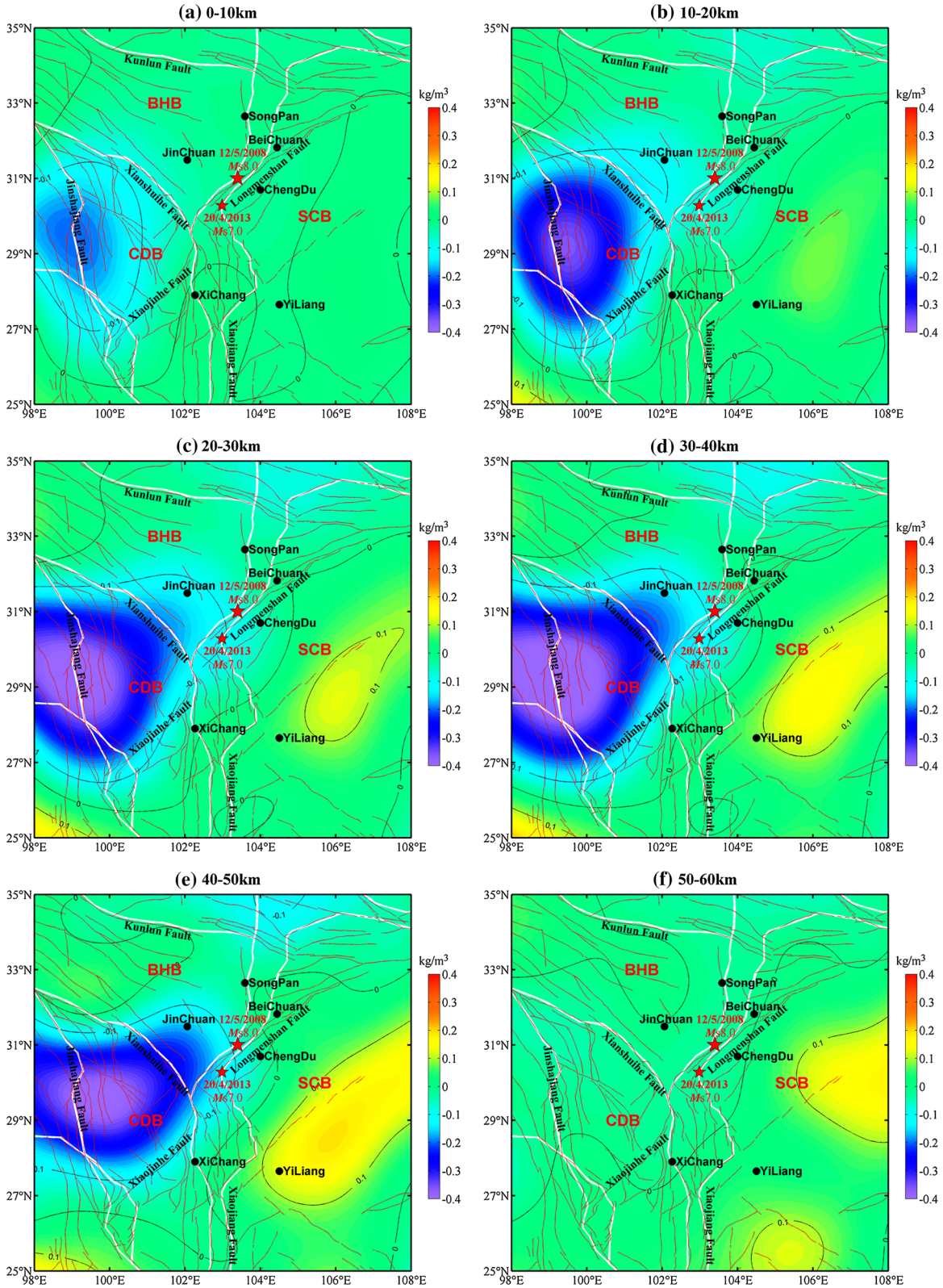

Fig. 4 DENV in 2011–2012 derived from Fig. 2b

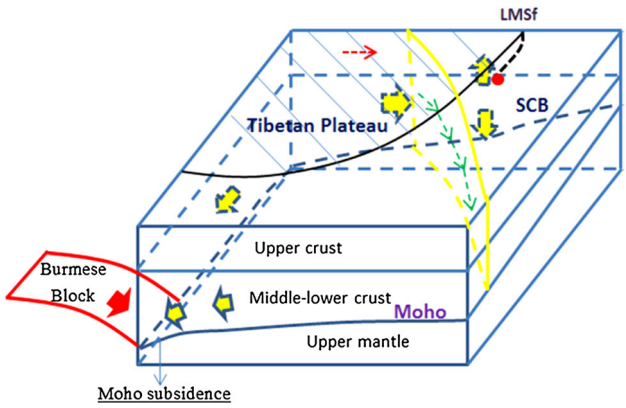

Fig. 5 Schematic crustal flow and Moho subsidence in the study area. The section outlined by *yellow lines* indicates the Xianshuihe fault section. The *red dashed arrow* indicates the eastward extrusion of the upper crust beneath the eastern Tibetan Plateau. The *red broad arrow* indicates the subduction of the Burmese block. The *yellow arrows* with *gray trim* indicate the direction of the middle-lower crust flow. The *green arrows* indicate the middle-lower crust flow along the Xianshuihe fault (Bai et al., 2010). The *red point* is the epicenter of the Lushan earthquake

mass, the subsurface environment would be dominated by pulling power caused by matter flow in different directions. Both Li (2010) and Zhang and Engdahl (2013) suggested that most earthquakes ($M_S \geq 7$) occurring on the margin of the Bayan Har block have been related to middle-lower crust flow. The Lushan earthquake may have been a case of the continuously decreasing DENV of the middle-lower crust.

In 2010–2011, the larger negative DENV of the middle-lower crust (Fig. 3b–e) beneath the Bayan Har block and both sides of the Xianshuihe fault, not appearing under the Sichuan basin, indicated that the expansive body was blocked by the Sichuan basin. Moreover, at the lower crust east of the Xiaojiang fault (Fig. 3e), the DENV was obviously negative. It it likely that the hot material flowed to this area from the Bayan Har block along the Xianshuihe fault, a channel of lower crust flow (Bai et al. 2010). At the same time, the movement of the middle-lower crust along the Xianshuihe fault dragged the upper crust of the south segment of the Longmenshan fault area and made the stress accumulate, supported by the findings of Shan et al. (2013) based on Coulomb failure stress. In Fig. 4b, c, comprising 2010–2011, the DENV of the middle-lower crust still continued to decrease markedly on both sides of the Xianshuihe fault in 2011–2012. More importantly, the weak crust of the Bayan Har block and Chuan-Dian block (Clark and Royden 2000) was a requirement for the subsurface expansion. Then the ongoing expansion blocked by the rigid Sichuan basin accumulated the stress at the southwest segment of the Longmenshan fault.

Shan et al. (2013) found that the Coulomb failure stress increased with time on the Xianshuihe fault after the Wenchuan earthquake, 2008. Unlike the Wenchuan earthquake, the Lushan earthquake and its aftershocks occurred in a high Poisson ratio region (Zheng et al. 2013). More strain energy could be absorbed by deformation in the lateral direction. To be dragged by the continuous movement of the middle-lower crust, the stress and strain of the upper crust in the southwest segment of the Longmenshan fault exceeded the threshold value and generated the Lushan earthquake. The larger negative DENV at the lower crust crossed over the southwest segment of the Longmenshan fault with a NW-SE trend (Fig. 4c–e). Does this indicate that the accumulation of stress and strain of the lower crust reached the threshold? According to Yang and Liu (2009), the lower crustal flow is faster than the surface deformation, which may have led to the occurrence of the Lushan earthquake.

Zhang et al. (2011) suggested that the Jinshajiang fault was an abrupt change belt of the eastward flow of the lower crust. Meanwhile, the DENV of both sides of the Jinshajiang fault changed from positive in 2010–2011 (Fig. 3a–e) to negative in 2011–2012 (Fig. 4a–e). This is not a suitable condition for accumulation of stress and strain. Adding the DENV of the two periods, we can see that the DENV can be canceled out except in the southwest region of the Chuan-Dian block in the 40–50-km layer. This may be controlled by the interactions between the Tibetan Plateau, Burmese block and Chuan-Dian block. The counterbalanced DENV in the Chuan-Dian block indicated that the accumulative DENV was very small from 2010 to 2012. The remaining positive DENV in the area of the southwest Chuan-Dian block should have been caused by discontinuous eastward subduction beneath the Eurasian plate of the Burmese block (e.g., Huang and Zhao 2006; Li et al. 2008).

The thickening of the Tibetan crust with time includes the Moho subsidence as well as surface uplift (Sun et al. 2009). As shown in Fig. 5, the eastward subduction of the Burmese block may sink the Moho surface beneath the southwest margin of the Chuan-Dian block. Then the partial melting under the Tibetan Plateau should flow toward the southwest and the DENV decrease as shown in Figs. 3e and 4e. The upper crust may move southwest following the middle-lower crust. This is consistent with result of Wang et al. (2008) obtained from GPS observations. It would speed up the southward and southwestward flow beneath the southwest segment of the Longmenshan fault, making the middle-lower crust beneath the Bayan Har block expand and then accumulate stress by the interaction between the brittle upper crust and rheological middle-lower crust. Based on previous studies (Li and Fu 1983; Zhu et al. 1985) and the continuous larger negative DENV around the

epicenter (Fig. 4c–e), we suggested that the Moho subsidence may provide another major impetus to earthquakes.

In this study, we obtained the DENV in the eastern Tibetan Plateau from 2010 to 2012 before the Lushan earthquake. The inversion results indicate that the middle-lower crust flow of the Tibetan plateau and Moho subsidence beneath the southwest margin region of the Chuan-Dian block may have induced the occurrence of the Lushan earthquake.

We have discussed the characteristics of subsurface density variations and analyzed the possible cause of the Lushan earthquake. It must be emphasized that the mechanism of the earthquake is rather complex and difficult to explain using a model or method. Our future work will examine many data and develop a suitable model to explain the preparation progress of strong earthquakes.

Acknowledgments We thank Gravity Network Center of China (GNCC) who provides the gravity data. This study was supported by the National Natural Science Foundation of China (41304060), the National Key Basic Research Program of China (973 Program, 2013CB733305) and Scientific Investigation of April 20, 2013 M7.0 Lushan, Sichuan Earthquake.

References

Bai DH, Unsworth MJ, Meju MA, Ma XB, Teng JW, Kong XR, Sun Y, Sun J, Wang LF, Jiang CS, Zhao CP, Xiao PF, Liu M (2010) Crustal deformation of the eastern Tibetan plateau revealed by magnetotelluric imaging. Nat Geosci 3(5):358–362

Barbosa VCF, Silva JBC (1994) Generalized compact gravity inversion. Geophysics 59(1):57–68

Battaglia M, Segall P, Roberts C (2003) The mechanics of unrest at Long Valley caldera, California. 2. Constraining the nature of the source using geodetic and micro-gravity data. J Volcanol Geotherm Res 127:219–245

Chatterjee S, Goswami A, Scotese CR (2013) The longest voyage: tectonic, magmatic, and paleoclimatic evolution of the Indian plate during its northward flight from Gondwana to Asia. Gondwana Res 23:238–267

Chen YT, Gu HD, Lu ZX (1979) Variations of gravity before and after the Haicheng earthquake, 1975, and the Tangshan earthquake, 1976. Phys Earth Planet Int 18:330–338

Chen Z, Lin BH, Bai WM, Cheng X, Wang YS (2011) A study on the influence of the 2008 Wenchuan earthquake on the stability of the Qinghai-Tibet Plateau tectonic block system. Tectonophysics 510:94–103

Clark MK, Royden LH (2000) Topographic ooze: building the eastern margin of Tibet by lower crustal flow. Geology 28(8):703–706

Clark MK, Bush JWM, Royden LH (2005) Dynamic topography produced by lower crustal flow against rheological strength heterogeneities bordering the Tibetan Plateau. Geophys J Int 162:575–590

Gan WJ, Zhang PZ, Shen ZK, Niu ZJ, Wang M, Wan YG, Zhou DM, Cheng J (2007) Present-day crustal motion within the Tibetan Plateau inferred from GPS measurements. J Geophys Res 112:B08416

Hao H T, Hu M Z, Zheng B, Wang T Q, Liang W F (2015) Gravity variation observed by scientific expedition of Lushan earthquake. J. Geodes. Geodyn., (In press)

Hao M, Wang QL, Shen ZK, Cui DX, Ji LY, Li YH, Qin SL (2014) Present day crustal vertical movement inferred fromprecise leveling data in eastern margin of Tibetan Plateau. Tectonophysics 632:281–292

He CS, Dong SW, Santosh M, Chen XH (2014) Seismic structure of the Longmenshan area in SW China inferred from receiver function analysis Implications for future large earthquakes. J Asian Earth Sci 96:226–236

Houseman G, England P (1993) Crustal thickening versus lateral expulsion in the Indian-Asian continental collision. J Geophys Res 98:12233–12249

Huang JL, Zhao DP (2006) High-resolution mantle tomography of China and surrounding regions. J Geophys Res 111:B09305

Jacobsen BH (1987) A case for upward continuation as a standard separation filter for potential field maps. Geophysics 52(8):1138–1148

Jiang WL, Zhang JF, Tian T, Wang X (2012) Crustal structure of Chuan-Dian region derived from gravity data and its tectonic implications. Phys Earth Planet Int 212–213:76–78

Klemperer SL (2006) Crustal flow in Tibet: geophysical evidence for the physical state of Tibetan lithosphere, and inferred patterns of active flow. Geol Soc Lond Spec Publ 268(1):39–70

Last BJ, Kubik K (1983) Compact gravity inversion. Geophysics 48(6):713–721

Lei SX, Ran YK, Wang H, Chen LC, Li X, Wu FY, Han F, Liu CL (2014) Discussion on the whether there are coseismic surface ruptures of the Lushan M_S7.0 earthquake at Longmen area and its implications. Seismol Geol 36(1):266–274 (in Chinese with English abstract)

Li DW (2010) The regularity and mechanism of East Kunlun, Wenchuan and Yushu earthquakes and discussion on genesis and prediction of continental earthquakes. Earth Sci Front 17(5):179–192 (in Chinese with English abstract)

Li RH, Fu ZZ (1983) Local gravity variations before and after the Tangshan earthquake ($M = 7.8$) and the dilatation process. Tectonophysics 97(1–4):159–169

Li C, van der Hilst RD, Meltzer AS, Engdahl ER (2008) Subduction of the Indian lithosphere beneath the Tibetan Plateau and Burma. Earth Planet Sci Lett 274:157–168

Lu RQ, He DF, John S, Wu JE, Liu B, Chen Y (2014) Structural model of the central Longmen Shan thrusts using seismic reflection profiles: Implications for the sediments and deformations since the Mesozoic. Tectonophysics 630:43–53

Molnar P, Tapponnier P (1975) Cenozoic tectonics of Asia: effects of a continental collision. Science 189(4201):419–426

Royden LH, Burchfiel BC, van der Hilst RD (2008) The geological evolution of the Tibetan Plateau. Science 321:1054–1058

Shan B, Xiong X, Zheng Y, Jin BK, Liu CL, Xie ZJ, Hsu HT (2013) Stress changes on major faults caused by 2013 Lushan earthquake and its relationship with 2008 Wenchuan earthquake. Sci China Earth Sci 56(7):1169–1176

Shen CY, Li H, Sun SA, Liu SM, Xuan SB, Tan HB (2009) Dynamic variations of gravity and the preparation progress of the Wenchuan M_S8.0 earthquake. Chin J Geophys 52(10):2547–2557 (in Chinese with English abstract)

Shoenbohm LM, Burchfiel BC, Chen LZ (2006) Propagation of surface uplift, lower crustal flow, and Cenozoic tectonics of the southeast margin of the Tibetan Plateau. Geology 34(10):813–816

Sun WK, Wang Q, Li H, Wang Y, Okubo S, Shao DS, Liu DZ, Fu GY (2009) Gravity and GPS measurements reveal mass loss beneath

the Tibetan-Geodetic evidence of increasing crustal thickness. Geophys Res Lett 36:L02303

Tapponnier P, Peltzer G, Le Dain AY, Armijo R (1982) Propagating extrusion tectonics in Asia new insights from simple experiments with plasticine. Geology 10:611–616

Tapponieretal P, Xu ZQ, Roger F, Meyer B, Arnaud N, Wittlinger G, Yang JS (2001) Oblique stepwise rise and growth of the Tibet Plateau. Science 294:1671–1677

Wang CY (2003) Three-dimensional velocity structure of crust and upper mantle in southwestern China and its tectonic implications. J Geophys Res 108(B9):2442

Wang CY, Han WB, Wu JP, Lou H, Chan WW (2007) Crustal structure beneath the eastern margin of the Tibetan Plateau and its tectonic implications. J Geophys Res 112:B07307

Wang YZ, Wang EN, Shen ZK, Wang M, Gan WJ, Qiao XJ, Meng GJ, Li TM, Tao W, Yang YL, Cheng J, Li P (2008) GPS-constrained inversion of present-day slip rates along major faults of the Sichuan-Yunnan region. Sci China Earth Sci 51:1267–1283

Wang CY, Zhu LP, Lou H, Huang BS, Yao ZX, Luo XH (2010) Crustal thicknesses and Poisson's ratios in the eastern Tibetan Plateau and their tectonic implications. J Geophys Res 115:B11301

Xu XW, Wen XZ, Han ZJ, Chen GH, Li CY, Zheng WJ, Zhang SM, Ren ZQ, Xu C, Tan XB, Wei ZY, Wang MM, Ren JJ, He ZT, Liang MJ (2013) Lushan M_S7.0 earthquake: A blind reverse-fault event. Chin Sci Bull 58:3437–3443

Yang YQ, Liu M (2009) Crustal thickening and lateral extrusion during the Indo-Asian collision: a 3D viscous flow model. Tectonophysics 465:128–135

Zhan Y, Zhao GZ, Unsworth M, Wang LF, Chen XB, Li T, Xiao QB, Wang JJ, Tang J, Cai JT, Wang YZ (2013) Deep structure beneath the southwestern section of the Longmenshan fault zone and seimogenetic context of the 4.20 Lushan M_S7.0 earthquake. Chin Sci Bull 58:3467–3474

Zhang PZ, Engdahl ER (2013) Great earthquakes in the 21st century and geodynamics of the Tibetan Plateau. Tectonophysics 584:1–6

Zhang PZ, Shen ZK, Wang M, Gan WJ, Bürhmann R, Molnar P, Wang Q, Niu ZJ, Sun JZ, Wu JC, Sun HR, You XZ (2004) Continuous deformation of the Tibetan Plateau from Global Positioning System data. Geology 32(9):809–812

Zhang ZJ, Wang YH, Chen Y, Houseman GA, Tian XB, Wang E, Teng JW (2009) Crustal structure across Longmenshan fault belt from passive source seismic profiling. Geophys Res Lett 36:L17310

Zhang ZJ, Deng YF, Teng JW, Wang CY, Gao R, Chen Y, Fan WM (2011) An overview of the crustal structure of the Tibetan plateau after 35 years of deep seismic soundings. J Asian Earth Sci 40:977–989

Zhao CP, Zhou LQ, Chen ZL (2013) Source rupture process of Lushan M_S7.0 earthquake, Sichuan, China and its tectonic implications. Chin Sci Bull 58:3444–3450

Zheng Y, Ge C, Xie ZJ, Yang YJ, Xiong X, Hsu HT (2013) Crustal and upper mantle structure and the deep seismogenic environment in the source regions of the Lushan earthquake and the Wenchuan earthquake. Sci China Earth Sci 56(7):1158–1168

Zhu YQ, Wu B, Xing RY (1985) Gravity variation and Moho surface deformation before and after 1976 Tangshan earthquake. Acta Seismologica Sinca 7(1):57–73 (in Chinese with English abstract)

Zhu YQ, Zhan FB, Zhou JC, Liang WF, Xu YM (2010) Gravity measurements and their variations before the 2008 Wenchuan earthquake. Bull Seismol Soc Am 100(5B):2815–2824

Zhu YQ, Wen XZ, Sun HP, Guo SS, Zhao YF (2013) Gravity changes before and the Lushan, Sichuan, $M_S = 7.0$ earthquake of 2013. Chin J Geophys 56(6):1887–1894 (in Chinese with English abstract)